DNA Cytosine C^5 Methyltransferase Dnmt1: Catalysis-Dependent Release of Allosteric Inhibition†

Željko M. Svedružić‡ and Norbert O. Reich*

Department of Chemistry and Biochemistry, University of California, Santa Barbara, California 93106

Received February 17, 2005; Revised Manuscript Received May 2, 2005

ABSTRACT: We followed the cytosine C^5 exchange reaction with Dnmt1 to characterize its preference for different DNA substrates, its allosteric regulation, and to provide a basis for comparison with the bacterial enzymes. We determined that the methyl transfer is rate-limiting, and steps up to and including the cysteine−cytosine covalent intermediate are in rapid equilibrium. Changes in these rapid equilibrium steps account for many of the previously described features of Dnmt1 catalysis and specificity including faster reactions with premethylated DNA versus unmethylated DNA, faster reactions with DNA in which guanine is replaced with inosine [poly(dC-dG) vs poly(dI-dC)], and 10−100-fold slower catalytic rates with Dnmt1 relative to the bacterial enzyme M.HhaI. Dnmt1 interactions with the guanine within the CpG recognition site can prevent the premature release of the target base and solvent access to the active site that could lead to mutagenic deamination. Our results suggest that the β-elimination step following methyl transfer is not mediated by free solvent. Dnmt1 shows a kinetic lag in product formation and allosteric inhibition with unmethylated DNA that is not observed with premethylated DNA. Thus, we suggest the enzyme undergoes a slow relief from *allosteric inhibition* upon initiation of catalysis on unmethylated DNA. Notably, this relief from allosteric inhibition is not caused by self-activation through the initial methylation reaction, as the same effect is observed during the cytosine C^5 exchange reaction in the absence of AdoMet. We describe limitations in the Michaelis−Menten kinetic analysis of Dnmt1 and suggest alternative approaches.

DNA methylation in eukaryotes occurs predominately at CpG dinucleotides and is essential for normal embryogenesis and cellular activity (*1*). The patterns of DNA methylation are tissue-specific and change dynamically throughout development. Inappropriate DNA methylation of tumor suppresser genes (*2*) and DNA repair genes (*3*−*5*) are nonmutagenic events that occur early in carcinogenesis (*6*). Dnmt1[1] is one of three predominant isoforms and has both de novo and maintenance activity in vitro and in vivo. Dnmt1 is a large multidomain protein that is structurally and functionally more complex than its smaller, bacterial counterparts (*7*−*15*). Mechanism-based inhibition of bacterial and mammalian DNA cytosine methyltransferases by 5-fluorocytosine (*14*, *16*), and the conserved sequence motifs observed in all DNA cytosine methyltransferases (*17*, *18*), suggest that Dnmt1 and its bacterial counterparts share similar catalytic mechanisms (Figure 1). However, the sequence homology with the bacterial enzymes is found only in the small C terminal domain of Dnmt1 (*18*), and the large N terminal domain contains numerous regulatory sites, including a site of phosphorylation (Ser 514) (*19*), an allosteric DNA binding site (*8*, *20*), nuclear localization signal (*21*), PCNA binding sequence (*22*), replication foci homing sequence (*23*), and Zn-finger sequence motifs (*20*). The N-terminal allosteric site is believed to regulate the enzyme's preference for DNA containing a distribution of 5-methylcytosines (premethylated DNA) (*11*, *20*). An N-terminal allosteric site was postulated to cause potent cell-based, sequence-dependent Dnmt1 inhibition (*8*). The majority of the reported mechanistic studies on mammalian Dnmt1 use the murine (*7*−*10*, *24*) and human (*11*, *12*, *14*) enzymes, which share 78% sequence identity.

Dnmt1's preference for premethylated DNA is frequently invoked as a key regulatory mechanism (*7*, *10*−*13*, *25*). Premethylated DNA includes sequences in which cytosine within the CpG dinucleotide in duplex DNA is methylated (hemimethylated DNA) and in which the 5-methylcytosine lies outside this recognition CpG but within the enzyme's DNA footprint. Hemimethylated DNA occurs predominately following DNA replication and provides a basis for Dnmt1's propagation of methylation patterns, presumably through a multiprotein complex that assembles at the sites of replication (*22*). 5-Methylcytosines (^{5m}C) positioned outside the target CpG dinucleotide are thought to be important for the allosteric regulation of the enzyme.

† This work was supported by NIH GM56289 to N.O.R.

* To whom correspondence should be addressed. E-mail: reich@chem.ucsb.edu; phone 805-893-8368; fax 805-893-4120.

‡ Current address: School of Molecular Biosciences, Department of Biophysics and Biochemistry, Washington State University, Pullman, WA 99164.

[1] Abbreviations: AdoMet, *S*-adenosyl-L-methionine; AdoHcy, *S*-adenosyl-L-homocysteine; bp, base pair, as two bases paired in Watson−Crick fashion; C, cytosine; C^5 or C^6, etc., carbon 5 or carbon 6 in a pyrimidine ring; ^{5m}C, 5-methylcytosine; dCTP, deoxycytosine triphosphate; dITP, deoxyinosine triphosphate; Dnmt1, DNA methyltransferase type 1; MEL, mouse erythroleukemia; M.HhaI, methyltransferase, *Haemophilus haemolyticus* type I; poly(dG-dC) or dGdC, double-stranded alternating polymer of deoxyguanine and deoxycytosine; poly-(dI-dC), double-stranded polymer of alternating deoxyinosine-deoxycytosine; pm-poly(dG-dC) or pm-dGdC, double-stranded alternating polymer of deoxyguanine and deoxycytosine; pm-poly(dI-dC), premethylated poly(dI-dC); sin, sinefungin; SKIE, solvent kinetic isotope effect.

10.1021/bi050295z CCC: $30.25 © 2005 American Chemical Society
Published on Web 06/16/2005

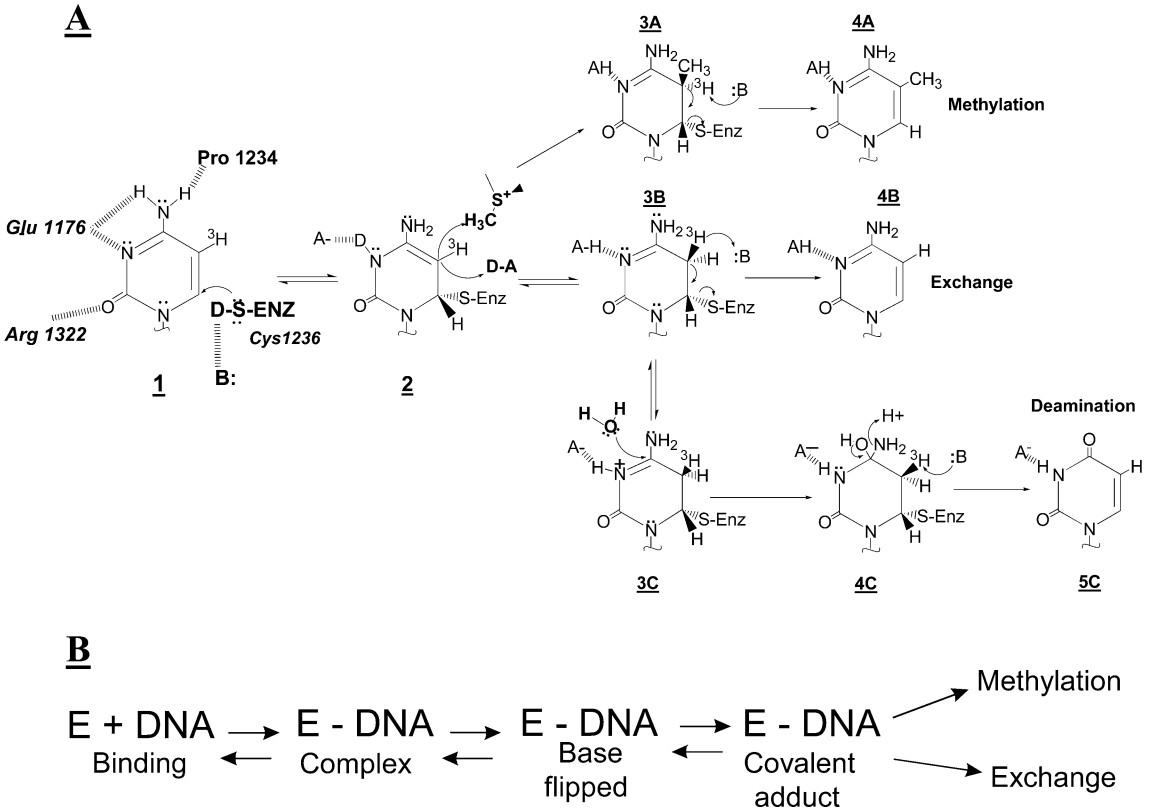

FIGURE 1: (A) Reactions catalyzed by cytosine C^5 DNA methyltransferases: methylation (A) exchange (B) and deamination (C) (*44*). The target cytosine interacts with active site residues (**1**) to facilitate cysteine nucleophilic attack at the C^6 position. Nucleophilic attack disrupts the pyrimidine's aromaticity, generating the reactive covalent adduct (**2**). Intermediate **2** can readily undergo electrophilic addition, either through methylation (**3A**) or protonation (**3B**). **3B** can lead to the exchange reaction (**4B**) or to mutagenic deamination (**3B** → **4C** → **5C**). Acidic groups are labeled as HA and basic groups are labeled as :B. All exchangeable protons that can result in a SKIE are shown as D in intermediates (**1** and **2**). The pre-steady-state in the methylation reaction are all steps leading to intermediate **3A** (or **3B** for exchange), while the steady state are subsequent steps (see methods). Conserved active site residues are indicated. (B) Four steps that control the target base attack by pyrimidine methyltransferases in a rapid equilibrium (*28*).

Dnmt1's catalytic preference for premethylated DNA derives in part from a faster methylation constant (*7*). Pedrali-Noy et al. postulated that the enzyme's preference for premethylated DNA is due to the inhibitory action of unmethylated DNA (*26*), which was further suggested to function through an allosteric site on the N-terminal domain (*20*). A variety of studies have shown that the N-terminal domain is required for Dnmt1 function (*11*, *27*). Removal of the first 501 N-terminal residues results in a mutant Dnmt1 with activities higher than WT with both unmethylated and premethylated DNA (*11*). Thus, some form of allosteric inhibition is likely to be present with all DNA substrates. Surprisingly, the N-terminal deletion mutant still differentiates between premethylated and unmethylated DNA (*11*). We previously showed that Dnmt1 forms ternary enzyme/DNA/DNA complexes, that different DNA sequences vary in their binding affinity, and that the binding of a second DNA molecule most likely involves the N-terminal domain (*8*, *9*). In sum, previous studies (*8*, *11*, *12*, *26*) suggest that the N-terminal domain acts to inhibit the enzyme and that a complex interplay between different DNA binding sites results in the enzyme's regulation. Our interest is to characterize the mechanisms of the enzyme's substrate preference and allosteric regulation.

We recently defined a kinetic approach for M.HhaI providing new insights into which steps limit catalysis and the nature of various reaction intermediates (*28*). Briefly, intermediate **2** (Figure 1) is readily protonated in the presence

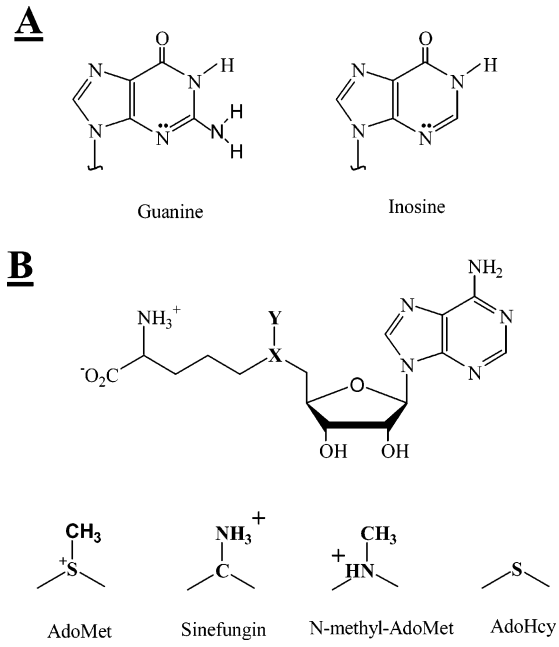

FIGURE 2: Inosine and guanine (A); AdoMet and its analogues (B).

of a proton donor ($pK_a = 11-18$; *29*), so the ^3H exchange reaction in the presence of AdoMet analogues (i.e., proton donors, Figure 2) represents an opportunity to analyze this crucial stage of catalysis (Figure 1, **1** → **2**). Intermediate **2** is most likely important for inhibitors of Dnmt1 like 5-aza-

cytosine, which was recently approved by the FDA to treat blood-related tumors (*30*), or zebularine which is in phase II clinical trials (*30*). Here we analyze intermediate **2** with murine Dnmt1, by monitoring the cytosine C^5 exchange reaction with AdoMet analogues and poly(dG-dC) and poly(dI-dC) substrates. Our primary interest is of the Dnmt1/DNA complex involving the cognate site, as represented either by poly(dG-dC) or poly(dI-dC). These homogeneous substrates cause each enzyme molecule to interact with the same DNA sequence, at both the active and the allosteric sites (Figure 10). Further, all enzyme−DNA complexes are likely to be active since every enzyme molecule bound to the DNA is bound at the recognition site, thereby increasing the sensitivity of the assay for an enzyme as slow as Dnmt1. These studies with poly(dG-dC) and poly(dI-dC) are conveniently compared with prior studies of Dnmt1 (*7*, *8*, *10*−*12*, *26*).

MATERIALS

S-Adenosyl-L-[methyl^{14}C] methionine (59 mCi/mmol or 131 cpm/pmol), *S*-adenosyl-L-[methyl ^{3}H] methionine (66−82 Ci/mmol or 6100−7200 cpm/pmol), deoxy[5-^{3}H] cytidine 5′ triphosphate (19.0 Ci/mmol) ammonium salt, and Sequenase 2.0 were purchased from Amersham Corp. Poly(dG-dC) 850 bp, poly(dI-dC) 1960 bp, dITP, and dCTP were purchased from Pharmacia Biotech. DTT, Trizma, BSA fraction V, and activated charcoal were purchased from Sigma Chemical Co. Some BSA batches were inhibitory, and each BSA batch was tested by showing that the reaction rate did not vary with BSA concentration (0.2−1.0 mg/mL). DE81 filters were purchased from Whatman, Inc. Sinefungin was purchased from Sigma Chemical Co. AdoMet 85% pure was purchased from Sigma Chemical Co. and further purified (*31*). Dnmt1 was prepared from mouse erythroleukemia cells as previously described (*32*), and its concentration was determined by active site titration (*7*) and by titration with a potent Dnmt1 inhibitor ($K_d \approx 30$ nM; *8*). The enzyme concentration determined by the pre-steady-state burst is 40% lower than the enzyme concentration determined by titration with the inhibitor. Because the pre-steady-state burst is expected to give a lower measure of enzyme concentration (eq 1), we relied on the use of the oligonucleotide inhibitor to determine Dnmt1 concentration. M.HhaI was expressed using *Escherichia coli* strain ER1727 containing plasmid pHSHW-5 (both provided by S. Kumar, New England Biolabs) and purified as previously described (*15*). The concentration of AdoMet, sinefungin, premethylated and unmethylated poly(dG-dC) and poly(dI-dC) were determined by absorbance at 260 nm. The respective molar absorptivity coefficients are 15.0×10^3 M^{-1} cm^{-1} for AdoMet and sinefungin (Merck Index), 6.9×10^3 M^{-1} cm^{-1} for poly(dI-dC) bp, 8.4×10^3 M^{-1} cm^{-1} for poly(dG-dC) bp (Pharmacia Tech. Info. Sheet).

METHODS

Preparation of Premethylated poly(dG-dC) and poly(dI-dC). The premethylated substrates were prepared with excess AdoMet and M.HhaI. The labeling reaction was run for only one or two turnovers (1.5−2 min) to limit the number of methylated cytosines (^{5m}C) to the number of initially bound M.HhaI molecules. For example, 30−40 μM M.HhaI and 100 μM of [methyl ^{14}C] AdoMet were incubated with 300 μM bp DNA (approximately 30 μM of binding sites for M.HhaI on the DNA substrate, based on a 10 bp footprint; Figure 10 and ref *33*). This reaction was quenched (90 °C water bath for 3−5 min), followed by slow cooling (2−3 h) to room temperature to ensure gradual annealing of self-complementary DNA. M.HhaI was removed by centrifugation, and the remaining labeling mixture was dialyzed against 10 mM Tris/HCl pH (8.0) and 10 mM EDTA. The extent of dialysis was determined with DE81 filter papers and washing the filters with 500 mM KPi buffer pH = 6.8. Dialysis was continued until the washed and unwashed samples had the same counts. The final DNA concentration and extent of methylation were determined by measuring the absorbance at 260 nm and ^{14}C radioactivity, respectively. The substrates prepared by this procedure contain an average of one ^{5m}C every 7 to 20 bp, depending on the length of the labeling reaction and the ratio between total M.HhaI and DNA. All substrates prepared in this fashion showed a characteristic pre-steady-state burst (*7*).

Preparation of [5-^{3}H] Cytosine-poly(dG-dC) and poly(dI-dC). Poly(dI-dC) was labeled by incubating 500 μM (bp) of poly(dI-dC) with 100 μM [5-^{3}H] dCTP, 1 mM CTP, 10 mM dITP with 0.62 U/μL of Sequenase 2.0 in 40 mM Tris/HCl (pH 7.5), 10 mM $MgCl_2$, 50 mM NaCl, 10 mM DTT and 1.0 mg/mL BSA. The same approach was used in the labeling reactions with poly(dG-dC) except that poly(dI-dC) and 10 mM dITP were replaced by poly(dG-dC) and 1 mM dGTP. The labeling reactions were run for 5 h at room temperature. Incorporation of [5-^{3}H] cytosine was determined by placing the reaction aliquots onto DE81 filter papers. Filters were washed twice for 5 min in 500 mM KPi buffer (pH 6.8) and dried under a heat lamp. The high ionic strength (500 mM KPi) removes free nucleotides from the DE81 filters without impacting the bound DNA. The extent of label incorporation was calculated by comparing the counts from unwashed and washed papers. The procedure routinely results in approximately 30−60% label incorporation. The quenching, annealing, and dialysis procedures were as described for the premethylated substrates. The removal of reaction components was determined by comparing the radioactivity from unwashed and washed DE81 papers as indicated above. The labeling gives 13−40 cpm/pmol of base pairs for poly(dI-dC) and 60−105 cpm/pmol of base pairs for poly(dG-dC).

Methylation Reactions. The methylation reactions were prepared by incubating Dnmt1, DNA substrate, and radioactive AdoMet in 100 mM Tris/HCl (pH, 8.0), 10 mM EDTA, 10 mM DTT, and 0.5 mg/mL of BSA at 37 °C. The enzyme and DNA concentrations are specific for each assay and described in the figure legends. Incorporation of tritiated methyl groups into DNA was determined as previously described (*31*). Briefly, a typical reaction was followed by placing reaction aliquots onto DE81 paper, in which case DNA methylation is detected as soon as the methyl group is transferred to DNA (Figure 1, **3A**). Thus, the pre-steady-state and steady-state rates are determined by the steps that lead to and follow formation of intermediate **3A** (Figure 1), respectively.

Tritium Exchange Reactions. The tritium exchange reaction was followed essentially as previously described (*34*). Briefly, tritium exchange is measured by quenching reaction aliquots in an acid suspension (HCl, pH = 2.0−2.5) of

activated charcoal. Because **3A** and **3B** (Figure 2) rapidly degrade in acid, their formation can be detected prior to release from the enzyme, thereby allowing the determination of kinetic constants up to and including the formation of **3A** and **3B**. The enzyme concentration, DNA concentration, and cofactor concentration are specific for each assay and described in the figure legends. All reactions were saturated with the cofactor. The reaction buffer was 100 mM Tris/HCl (pH, 8.0), 10 mM EDTA, 10 mM DTT, and 0.5 mg/mL of BSA.

Preparation of [5-^{3}H] Cytosine pm-poly(dG-dC) and pm-poly(dI-dC). ^{3}H-labeled premethylated DNA was prepared from [5-^{3}H] cytosine-poly(dG-dC) or [5-^{3}H] cytosine-poly(dI-dC) using the procedure described for the preparation of premethylated DNA.

Data Analysis. All reaction profiles were analyzed using the Microcal Origin 5.0 program. All rates were reported as the best fit values ± standard deviation. The burst profiles were fit to a two-step irreversible mechanism (*35*):

$$[P](t) = \alpha E_t(1 - e^{-k_{pss}t}) + E_t k_{ss} t \quad (1)$$

where $[P](t)$ is product at time t, E_t is total enzyme in the assay, α is a constant that relates the burst magnitude and the actual enzyme concentration, k_{pss} is the pre-steady-state rate constant, and k_{ss} is the lag transition rate constant. All initial velocity lags were analyzed using a model equation that represents two enzymes forms with different catalytic activities (*36*):

$$[P](t) = E_t k t - \frac{E_t k}{k_l}(1 - e^{-k_l t}) \quad (2)$$

where $[P](t)$ is product at time t, E_t is total enzyme in the assay, k is the catalytic rate constant, and k_l is the lag transition rate constant and corresponds to the transition rate between the inhibited and uninhibited forms. Unless otherwise indicated all other profiles were analyzed using a linear equation ($[P](t) = E_t k$; $[P](t)$ product at time t, E_t total enzyme, k turnover rate constant). Each experiment was repeated with different enzyme and substrate concentrations to test for the consistency in the observed phenomena; shown are representative examples.

SKIE Measurements. All experiments in D_2O buffers were measured in parallel with the corresponding H_2O experiments and were identical in all other parameters. The D_2O buffer was prepared as a 10-fold concentrate, and its pH was adjusted taking into account the pD vs pH correction (*37*) to be the same as in the corresponding H_2O buffer. H inventory profiles were analyzed using different forms of the Gross-Butler equation (*37*):

$$k_v^{D_2O} = k^{H_2O}\frac{(1 + v - v\phi^T)^n}{(1 + v - v\phi^G)^m} \quad (3)$$

where $k_v^{D_2O}$ is the measured rate constant when the fraction of D_2O is equal v, k^{H_2O} is the rate constant measured in pure H_2O, v is the fraction D_2O at which the rate constant was measured (i.e., 0.1, 0.2, 0.3, etc), and ϕ^T or ϕ^G are deuterium fractionation factors at the transition and the ground state, respectively (*37*). Different forms of eq 4 can be produced by changing the values for parameters n, m, as we described earlier (*28*).

Fluorescence Measurements. The equilibrium dissociation constant for the Dnmt1 CRE $a^F b^m$ complex was measured in the presence and absence of AdoMet by following changes in the intrinsic protein fluorescence as a function of increasing DNA concentration. The fluorescence was measured using a Perkin-Elmer LS50B instrument, with excitation at 290 nm (5 nm band-pass), and the emission at 340 nm (10 nm band-pass). To a first approximation an apparent dissociation constant (K_d) was calculated using the following equation:

$$\frac{F_o - F_i}{F_o - F_F} = \frac{(E_t - S_i + K_d) - \sqrt{(E_t - S_i + K_d)^2 - 4E_t S_i}}{2\cdot[E_t]} \quad (4)$$

where F_i is fluorescence at DNA concentration S_i, E_t is total Dnmt1 concentration, and F_O and F_F are the initial and the final fluorescence, respectively. The experimental data were analyzed by nonlinear least-squares fits using eq 4 and the Microcal Origin 5.0 program, with K_d, F_O, and F_F set as the free fit parameters. Prior to fitting using eq 4, the measured Dnmt1 fluorescence profiles were corrected for the inner filter effect that is caused by added DNA. The inner filter effect was measured by replacing Dnmt1 with free Trp at a concentration to get the same fluorescence as the initial Dnmt1 solution, using the following equation:

$$F_i = F_m + (F_o - F_w) \quad (5)$$

where F_i is the corrected florescence value that was used in the eq 4, F_m and F_w are measured Dnmt1 and free Trp fluorescence before the correction at a specific DNA concentration, and F_O is the initial fluorescence of the Dnmt1 (and free Trp) solution before addition of DNA or AdoMet. The correction curve showed that at the highest DNA concentration the inner filter effect was between 5 and 15% of the actual signal.

RESULTS

Pre-Steady-State and Initial Steady-State Methylation Reactions with poly(dI-dC) and pm-poly(dI-dC) (Figures 3A and 4A,C), poly(dG-dC) and pm-poly(dG-dC) (Figures 3B and 4B,C). Our initial interest was to characterize the methylation reaction (Figures 3A,B and 4A−C) with premethylated and unmethylated poly(dI-dC) and poly(dG-dC) substrates to provide a basis for a direct comparison with our recent study of M.HhaI (*28*) and prior studies of Dnmt1 with different DNA substrates (Table 1). The relatively fast reactions with poly(dI-dC) and pm-poly(dI-dC) allow the measurement of multiple turnovers (Figure 3A, Table 1). In contrast, the slow nonlinear reactions with poly(dG-dC) and pm-poly(dG-dC) limited our measurements to one or two turnovers, respectively (Figure 3B, Table 1). Both premethylated poly(dI-dC) and poly(dG-dC) show a mild pre-steady-state burst (Figure 3A,B) and no substrate inhibition (Figure 4C). Both unmethylated poly(dI-dC) and poly(dG-dC) show initial lags (Figure 3A,B), and increasing DNA concentrations leads to longer lags (Figure 3A,B) and greater substrate inhibition (Figure 4A,B). In summary, the premethylated and unmethylated substrates show distinct sub-

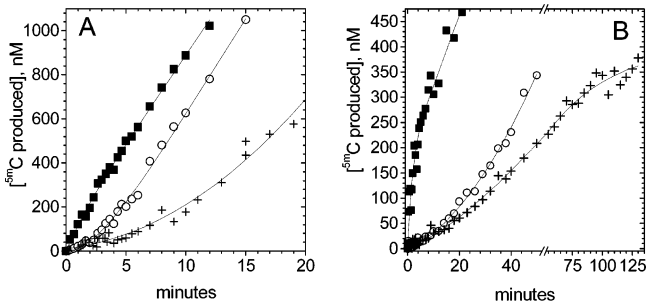

FIGURE 3: Dnmt 1 methylation reaction with different DNA substrates. (A) Methylation profiles (■) with pm-poly(dI-dC) (12 μM bp) and with poly(dI-dC) [12 μM bp (○) and 260 μM (+) bp] in the presence of 145 nM Dnmt1. pm-poly(dI-dC) has an average of one out of eight cytosines methylated. (B) Methylation profiles (■) with pm-poly(dG-dC) (10 μM bp) and with poly(dG-dC) [4 μM bp (○) and 20 μM (+) bp] in the presence of 270 and 350 nM Dnmt1, respectively. pm-poly(dG-dC) has an average of one out of seven cytosines methylated. All reactions were measured in the presence of 12.5 μM of AdoMet (6100 cpm/pmol).

strate inhibition characteristics and initial rates (Table 1). The catalytic rates measured with poly(dI-dC) are comparable to rates measured in previous studies (Table 1), demonstrating that this substrate provides a reliable basis to study Dnmt1. The catalytic rates with unmethylated and premethylated poly(dG-dC) are comparable to rates measured with other substrates with GC target sites (Table 1), suggesting that poly(dG-dC) is representative of such substrates.

The initial lag correlates with the extent of substrate inhibition (Figures 3 and Figure 4, and ref *26*). In general, features of both the assay design and inherent reaction mechanism can cause an initial lag during a normal reaction cycle (*36*, *38*). The lag is not due to our assay design since the lag is substrate-dependent and the lag is observed during methylation and exchange assays (Figures 3A,B and 5A,B). Preincubation of Dnmt1 with DNA for 10 min does not change the lag, changing Dnmt1 concentrations does not affect the lag, and changing the order of substrate addition (DNA and AdoMet) does not alter the lag. Thus, a slow ligand binding step does not cause the lag. A slow relief from enzyme inhibition is a well-known mechanism leading to a kinetic lag (*36*, *38*). In summary, we propose that for Dnmt1, the start of the catalytic action with the unmethylated substrate results in a slow relief from the allosteric inhibition causing an initial lag in the catalytic activity.

The lag transition rate constant and the subsequent catalytic rate constant (Table 1) can be calculated using the equation modeled on two enzyme forms whose interconversion is initiated at the start of catalysis (eq 2; *36*, *38*). The initial lag is only observed when the transition between the inhibited and uninhibited enzyme forms is slower than the catalytic rate (*36*, *38*). Thus, the lag is observed only in methylation (Figure 3) and during the exchange reaction with sinefungin (Figure 5), but not during the slow exchange reaction with *N*-methyl-AdoMet (data not shown). Finally, we also point out that saturation with poly(dG-dC) and poly(dI-dC) leads to partial inhibition (Figure 4A,B), indicating that occupancy of the allosteric site leads only to modulation, rather than complete loss of catalytic activity.

The premethylated substrate is similar to the substrate used in the original study which revealed differences in the initial lag and substrate inhibition (*26*). Interestingly, modifications in the ratio of ^{5m}C to C (^{5m}C/C) greater than 1:20 do not cause changes in the kinetic parameters (data not shown). This density of ^{5m}C corresponds to approximately one ^{5m}C per enzyme/DNA footprint (Figure 10A). This is consistent with our previous study showing that Dnmt1 has similar activities with premethylated substrates in which the distance between the target cytosine and ^{5m}C varies from 5 to 18 bp (*24*). The highest density between ^{5m}C and C sites was 1 to 7, to avoid problems associated with the potential depletion of the target cytosines. The pm-poly(dG-dC) and pm-poly(dI-dC) substrates show a mild pre-steady-state burst (Figure 3A,B), like the hemimethylated oligo substrates ((*7*) and Table 1).

The Exchange Reaction with AdoMet Analogues and Premethylated and Unmethylated poly(dG-dC) and poly(dI-dC) Substrates (Table 2 and Figure 5A,B). To analyze the enzyme's preference for premethylated DNA and its allosteric regulation, we used the cytosine C^5 exchange assay (Figure 1, **2** → **3B** → **4B**) and AdoMet analogues (*28*). The exchange rates are high with sinefungin, intermediate with *N*-methyl-AdoMet, and low with AdoHcy, and in the absence of the cofactor (Table 2). The AdoMet analogues used in this study differ only in the position that corresponds to the active methyl group on AdoMet (Figure 2), and the exchange rates correlate with the availability of proximal proton(s) in the position of the active methyl group. In summary, just as with M.HhaI (Table 2), the AdoMet analogues alter the exchange reaction by Dnmt1 by changing the rate-limiting proton transfer at the activated target base (Figure **2** → **3B**). Interestingly, the enzyme's DNA preferences are retained with AdoMet analogues that modulate the exchange reaction rate by over 3 orders of magnitude: the fastest exchange rates are observed with pm-poly(dI-dC), followed by poly(dI-dC), pm-poly(dG-dC), and poly(dG-dC) (Table 2). Thus,

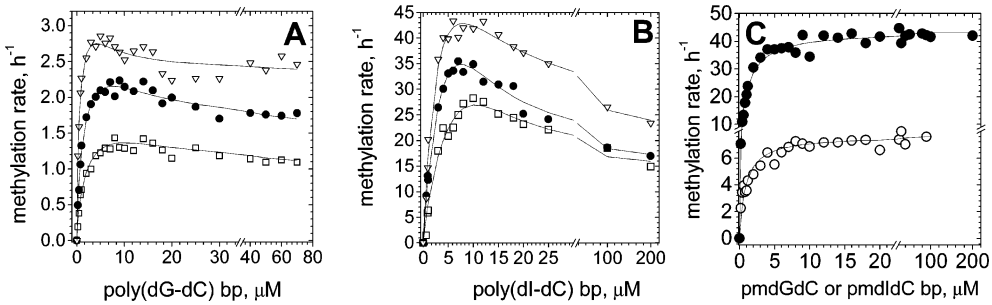

FIGURE 4: Methylation rate as a function of increasing concentration of substrate DNA. (A) poly(dG-dC) as the substrate and 80 nM (▽), 160 nM (●), and 250 nM (□) Dnmt1. (B) poly(dI-dC) as the substrate and 100 nM (▽), 200 nM (●), and 300 nM (□) Dnmt1. (C) pmpoly-(dI-dC) (●) and pmpoly(dG-dC) (○) as substrates and 100 nM Dnmt1.

Table 1: Dnmt1 Pre-Steady State and Steady-State Methylation Rates with Different DNA Substrates[a]

substrate	first turnover, h^{-1}	multiple turnovers, h^{-1}	conditions	references and enzyme source	comments
poly(dG-dC)	1.6 ± 0.6	*b*	4 μM bp, 15 μM AdoMet	Fig 3B, this study, mouse	Lag[d]: 1.2 ± 0.4 h^{-1}
	1 ± 0.3	0.2 ± 0.02	20 μM bp,15 μM AdoMet	Fig 3B, this study, mouse	Lag[d]: 0.7 ± 0.3 h^{-1}
pm-poly(dG-dC)	8.8 ± 0.6	5.1 ± 0.7	10 μM bp, 15 μM AdoMet	Fig 3B, this study, mouse	pre-steady state burst
poly(dI-dC)	*c*	37 ± 0.4	10 μM bp, 15 μM AdoMet	Fig 3A, this study, mouse	Lag[d]: 19.2 ± 1.2 h^{-1}
	c	20.6 ± 0.3	260 μM bp, 15 μM AdoMet	Fig 3A, this study, mouse	Lag[d]: 9.6 ± 0.6 h^{-1}
pm-poly(dI-dC)	56 ± 11	36 ± 0.5	12 μM bp, 15 μM AdoMet	Fig 3A this study, mouse	pre-steady state burst
poly(dI-dC)	*b*	20[e]	6.25 μM IC, 15 μM AdoMet	Fig 1 in (*7*), mouse	
poly(dI-dC)	*b*	26[e]	0.5 μM IC, 15 μM AdoMet	Fig 2A in (*8*), mouse	
poly(dI-dC)	*b*	70[e]	1 μM IC, 10 μM AdoMet,	Fig 4A in (*14*), human	
poly(dI-dC)	*b*	36[e]	1 μM IC, 10 μM AdoMet,	Fig 3A in (*14*), human	
-**CGG CGG CG**G-[f] -**GCC GCC GC**C-	0.85[e,g]		50 μM AdoMet, 1 μM CG, or 41 nM oligo	Fig 4A in (*12*), human	unmethylated GC rich oligo 36 bp
-MGG MGG MGG-[f] -**GCC GCC GC**C-	3.0[e,g]		10 μM AdoMet, 1 μM CG, or 83 nM oligo	Fig 4C in (*12*), human	hemimethylated GC rich oligo 36 bp
-**CGG CGG CG**G-[f] -**GCM GCM GC**M-	13.5[e,g]		10 μM AdoMet, 1 μM CG, or 41 nM oligo	Fig 6A in (*12*), human	premethylated GC rich oligo 36 bp
PRW3602 plasmid	1.5[e]	1.5[e]	10 μM AdoMet, 25 μM GC	Fig 1A in (*12*), human	unmethylated plasmid 2705 bp
-ATTGA**CG**TCAA-[f] -TAACT**GC**AGTT-	0.59 ± 0.02	*b*	15 μM oligo, 15 μM AdoMet	Table 3 in (*7*), mouse	unmethylated 30 bp oligo CG site in AT rich sequence
-ATTGA**MG**TCAA-[f] -TAACT**GC**AGTT-	3.0 ± 0.2	0.6 ± 0.05	15 μM oligo, 15 μM AdoMet	Fig 4 in (*7*), mouse	hemimethylated 30 bp oligo CG site in AT rich sequence; pre-steady state burst
-AGGGG**CG**GGGC-[f] -TCCCC**GC**CCCG-	0.15 ± 0.02	*b*	15 μM oligo, 15 μM AdoMet	Table 3 in (*7*), mouse	unmethylated 30 bp oligo CG site in GC rich sequence
-AGGGG**CG**GGGC-[f] -TCCCC**GM**CCCG-	1.2 ± 0.1	*b*	15 μM oligo, 15 μM AdoMet	Table 3 in (*7*), mouse	hemimethylated 30 bp oligo CG site in GC rich sequence; pre-steady state burst

[a] The present rates are measured at DNA and AdoMet concentrations that give the highest rates. In compiling the table, we did not use reported k_{cat} values, since different publications used different procedures to calculate those values, which can lead to large variations in otherwise comparable reactions (see appendix). [b] Not measured. [c] Cannot be calculated due to initial lag. [d] Lag transition rate as defined in eq 2 k_l. [e] The values were estimated from the actual data figures, and thus we cannot show error. [f] M stands for ^{5m}C, and methylation target sites are shown in bold. [g] Not enough information available to differentiate between turnovers. The table shows results only from Dnmt1 studies that gave enough experimental description (enzyme and substrate concentration, product conentration) to allow independent evaluation.

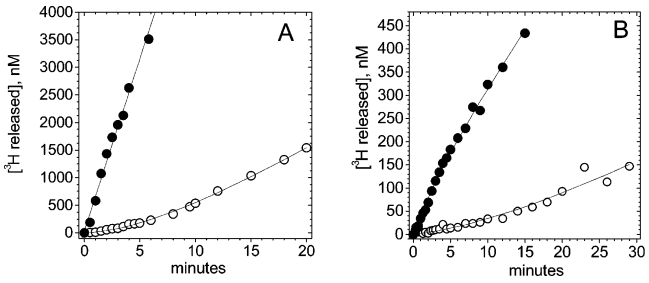

FIGURE 5: Tritium exchange reaction in the presence of sinefungin with different DNA substrates. (A) The exchange reaction with 105 nM Dnmt1, 20 μM of sinefungin, and 10 μM bp of ^{3}H-pmpoly-(dI-dC) (●) 19 cpm/pmol, ^{5m}C:C = 1:14, or ^{3}H-poly(dI-dC) (○), 33 cpm/pmol. (B) The exchange reaction with 160 nM Dnmt1, 20 μM of sinefungin, and 8 μM bp of ^{3}H-pmpoly(dG-dC) (●) 56 cpm/pmol, ^{5m}C:C = 1:15, or 8 μM bp of ^{3}H-poly(dG-dC) (○) (88 cpm/pmol).

differences between premethylated and unmethylated DNA, or between poly(dI-dC) and poly(dG-dC), do not derive from differences in the methyltransfer (Figure 1, **2** → **3A**) or proton-transfer rates (Figure 1, **2** → **3B**).

The exchange reaction with sinefungin is particularly revealing. First, an initial lag is observed in the absence of any production of ^{5m}C (Figure 5). Importantly, this shows that the increased rate following the initial lag in the methylation reaction (Figure 3A,B) cannot be due to self-activation through the AdoMet-dependent production of ^{5m}C at the start of catalysis. Also, the *steady-state* exchange rate constants for poly(dI-dC) and pm-poly(dI-dC) (Figure 5, Table 2) differ by 9-fold, in contrast to the nearly identical AdoMet-dependent methylation rates (Figure 3A, Table 1). Furthermore, the apparent $K_m^{sinefungin}$ measured with poly(dI-dC) is 9 times higher than with pm-poly(dI-dC) (5.1 ± 1.4 vs 0.6 ± 0.1 μM). For comparison, K_m^{AdoMet} in the methylation reaction with poly(dI-dC) is two times higher than with pm-poly(dI-dC) (1.3 ± 0.21 vs 2.7± 0.4 μM). Thus, these results indicate that studies of steps prior to methyltransfer (Figure 1, **2** → **3A**) can reveal unique insights into the enzyme's preference for different DNA substrates.

Tritium Release Rates during the AdoMet-Dependent Methylation Reaction with Premethylated and Unmethylated poly(dG-dC) and poly(dI-dC) Substrates (Figure 6A−C). We sought to determine the basis of Dnmt1's sinefungin-

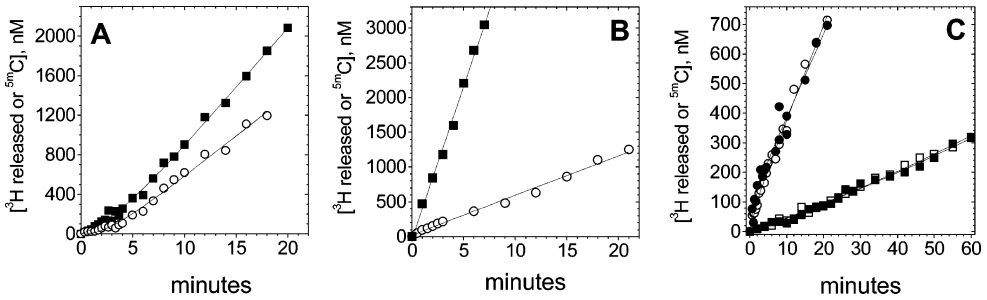

FIGURE 6: Methylation and tritium release profiles in the reaction with different DNA substrates. (A) Methylation (○) and tritium release (■) profiles with 12 μM bp ^{3}H-poly(dI-dC) (33 ± 2 cpm/pmol of bp) and 125 nM Dnmt1. (B) Methylation (○) and tritium release (■) with 12 μM bp ^{3}H-pmpoly(dI-dC) (19 ± 1.3 cpm/pmol of bp, ^{5m}C:C = 1:14) and 125 nM Dnmt1. (C) Methylation (●) and tritium release (○) profiles with 8 μM bp ^{3}H-pmpoly(dG-dC) (76 ± 5 cpm/pmol of bp, ^{5m}C:C = 1:17); methylation (■) and tritium release (□) profiles with 8 μM bp ^{3}H-poly(dG-dC) (102 ± 8 cpm/pmol of bp). The reactions with poly(dG-dC) and pmpoly(dG-dC) had 250 nM Dnmt1. All of reactions had 12.5 μM [^{14}C-methyl] AdoMet (131 cpm/pmol).

Table 2: (A) Exchange Rates with Unmethylated and Premethylated poly(dG-dC) and poly(dI-dC) with AdoMet Analogues and in the Absence of the Cofactor, for Dnmt1 and Small Bacterial Enzyme M.HhaI (*28*) and (B) Methylation and accompanying tritium release rates for Dnmt1 and bacterial enzyme M.HhaI (*28*)

(A)

	sinefungin rates, h^{-1}	*N*-methyl-AdoMet rates h^{-1}	AdoHcy rates, h^{-1}	no cofactor rates, h^{-1}
		Dnmt1 Exchange Rates, This Study		
poly(dG-dC)	3.5 ± 0.8	0.1 ± 0.02	<0.01	0.02 ± 0.001
poly(dI-dC)	42 ± 6	0.9 ± 0.1	0.1 ± 0.02	0.18 ± 0.02
pm-poly(dG-dC)	21 ± 4	0.5 ± 0.2	0.2 ± 0.05	0.08 ± 0.01
pm-poly(dI-dC)	438 ± 18	9 ± 0.8	2 ± 0.4	4.4 ± 0.5
		M.HhaI exchange rates [a]		
poly(dG-dC)	500 ± 200 44 ± 3[b]	33 ± 5	0.1 ± 0.02	650 ± 200 105 ± 10[b]
poly(dI-dC)	165 ± 20	145 ± 15	0.5 ± 0.005	10 ± 1

(B)

	Dnmt1		M.HhaI	
	methylation rates, h^{-1}	exchange rates, h^{-1}	methylation rates, h^{-1}	exchange rates, h^{-1}
poly(dG-dC)	1.7 ± 0.4	1.5 ± 0.3	140 ± 20 40 ± 4[b]	146 ± 15 43 ± 4[b]
poly(dI-dC)	37 ± 0.4	60 ± 2	65 ± 8	230 ± 25
pm-poly(dG-dC)	8 ± 0.6	8.4 ± 0.6		
pm-poly(dI-dC)	36 ± 0.5	257 ± 8		

[a] M.HhaI shows no difference between premethylated and unmethylated substrates prepared for this study. [b] Pre-steady-state and steady-state values, respectively.

dependent preference for pm-poly(dI-dC), which is not revealed during methylation (Figure 3 vs Figure 5). Accordingly, we measured the methylation and accompanying tritium release reactions simultaneously (Figure 6A−C) using ^{14}C-AdoMet and DNA substrates labeled with tritium at the C^5 position. On the basis of the reaction mechanism, every methyltransfer (Figure 1, **2** → **3A**) is expected to result in one tritium release (Figure 1, **3A** → **4A**) and the methylation and the accompanying tritium release rates are expected to be identical (*28*, *34*). We observe this 1:1 stoichiometry in both the pre-steady-state and steady-state methylation reactions with poly(dG-dC) and pm-poly(dG-dC) (Figure 6C and Table 2). Thus, intermediate **2** (Figure 1) leads only to methyltransfer (Figure 1, **2** → **3A**) with poly(dG-dC) and pm-poly(dG-dC) substrates. In contrast, Dnmt1 like M.HhaI (Table 2) shows an excess release of tritium during the AdoMet-dependent methylation of poly(dI-dC) and pm-poly(dI-dC) (Figure 6A,B and Table 2). The faster tritium release in the methylation reaction during the first turnover indicates that proton transfer at C^5 (Figure 1, **2** → **3B**) can take place before the methyltransfer step (Figure 1, **2** → **3A**) (*28*). Furthermore, since a single target base attack can result in only one tritium release (Figure 1, **2** → **3B** → **4B**), the severalfold difference between the tritium release and the methylation rates indicates that the enzyme can attack and release several bases prior to catalyzing one methyl transfer (*28*). Thus, the target base activation (Figure 1, **1** → **2**) is fast, and there is a direct competition between the target base release (i.e., breakdown of intermediate **1**) and the rate-limiting methyltransfer step (**2** → **3A**, Figure 1). The difference between poly(dI-dC) and pm-poly(dI-dC) (Figure 6A vs 6B) indicates that intermediate **2** (Figure 1, **1** → **2**) is formed faster with pm-poly(dI-dC) as already indicated by the data in Figure 5.

H Inventory Studies (Figure 7A,B). The rate-limiting step during the Dnmt1 exchange reaction with different DNA substrates and AdoMet analogues (Table 2) is proton transfer at the C^5 position, despite catalytic rates differing by 10−100-fold. We used H inventory studies to test whether the exchange reaction with sinefungin and different DNA substrates share the same rate-limiting step and catalytic intermediates despite large differences in the catalytic rates

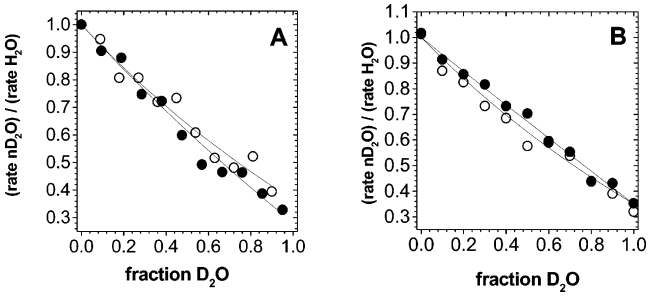

FIGURE 7: H inventory profiles during the exchange reaction with sinefungin and different DNA substrates. (A) The H inventory profiles for the exchange reaction with 10 μM bp poly(dG-dC) (○) and 10 μM bp premethylated poly(dG-dC) (●) in the presence of 20 μM sinefungin and 250 nM Dnmt1. The rates in H_2O and D_2O mixtures were measured during the first catalytic turnover (Figure 3B). (B) The H inventory profiles for the exchange reaction with 10 μM bp poly(dI-dC) (○) and 10 μM bp premethylated poly(dI-dC) (●) in the presence of 20 μM sinefungin and 250 nM Dnmt1. The rates in H_2O and D_2O mixtures were measured in the linear part of the reaction during multiple turnovers (Figure 3A). The data in both panels were analyzed using eq 3 as indicated in the text.

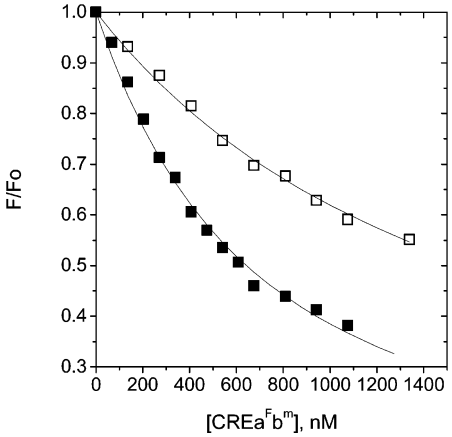

FIGURE 8: Fluorescence titration of Dnmt 1 with CRE a^Fb^M substrate. Equilibrium dissociation constant between 150 nM of Dnmt1 and increasing concentration of CRE a^Fb^m was measured in the presence of 12.5 μM of AdoMet (■), and in the absence of the cofactor (□) (100 mM Tris/HCl pH = 8.0, 10 mM EDTA, 10 mM DTT). Dnmt1 intrinsic fluorescence was measured in a microcuvette (sample slot 2 mm wide, 10 mm long) using a Perkin-Elmer LS50B fluorimeter at 25 °C. The total sample volume was 220 μL. The excitation was set at 290 nm (5 nm slit band-pass), and the emission was monitored at 335 nm (10 nm band-pass). The profiles were analyzed using the eqs 4 and 5.

(Figure 7A,B). Proton inventory profiles are rate studies performed at varying D_2O and H_2O ratios (*37*) and are very sensitive to the reaction mechanism (*28*).

Using the Gross-Butler equation (eq 5; *37*), we found that for all four DNA substrates the transition state fractionation factor (ϕ^T) is between 0.32 and 0.35 (0.35 ± 0.03 poly(dI-dC); 0.30 ± 0.05 pm-poly(dI-dC); 0.34 ± 0.04 poly(dG-dC); 0.30 ± 0.05 pm-poly(dG-dC)). The ground-state fractionation factor (ϕ^G) is between 2.1 and 2.4 [2.5 ± 0.2 poly(dI-dC); 2.5 ± 0.3 pm-poly(dI-dC); 2.3 ± 0.3 poly(dG-dC); 2.5 ± 0.3 pm-poly(dG-dC)]. The similar ϕ^T values suggest that reactions with the four different DNA substrates share the same rate-limiting step, while the similar ϕ^G values suggest that the reactions also share similar intermediates (*37*). The measured ϕ^T values are expected for reactions involving N−H−C proton bridges in the transition state (p 86 in ref *37*). A N−H−C proton bridge could form between the amino group on sinefungin (Figure 2) and intermediate **2** (Figure 1) if the rate-limiting step is proton transfer from the cofactor to the carbon 5 (Figure 1, **2** → **3B**) as we suggested earlier (Table 2 and ref *28*). Finally, the calculated ϕ^T and ϕ^G values are very similar to the values observed with M.HhaI (*28*), indicating that Dnmt1 and M.HhaI share similar proton inventory profiles in the exchange reaction with sinefungin. In summary, the proton inventory analysis indicates that Dnmt1's exchange reaction with different DNA substrates, as well as the exchange reaction by Dnmt1 and M.HhaI, can share the same intermediates and the rate-limiting step (Figure 1) even though the catalytic rates can vary by orders of magnitude (Table 2).

Fluorescence Titration of Dnmt1 with CRE a^Fb^m oligo (Figure 8). AdoMet binding by M.HhaI leads to a large conformational change, an increase in DNA binding affinity by 3 orders of magnitude (*15*), and a change in the mechanism of the target attack (*28*). We sought to determine if similar cofactor-mediated changes occur with Dnmt1. Dnmt1 interacts with hemimethylated DNA to form a 1:1 complex (*7, 9*), and replacing the target cytosine with 5-fluorocytosine (5FC) causes the methyl transfer (**2** → **3A**, Figure 1) to be slowed considerably. Thus, 5FC provides an opportunity to investigate how AdoMet alters Dnmt1−DNA interactions when the enzyme is trapped in the form of transient catalytic intermediates **1** and **2** (Figure 1; *39*). The DNA substrate was a 30-bp-long hemimethylated CRE ab^m substrate (*7*), and the binding was measured by following changes in intrinsic protein fluorescence as a function of increasing DNA concentration (see methods). The change in protein fluorescence caused by the Dnmt1−CREa^Fb^m interaction can be described as an apparent dissociation constant of 1.56 ± 0.2 μM and 0.6 ± 0.08 μM (eq 4) for binding in the presence and in the absence of AdoMet, respectively. These values are very similar to the previous dissociation constants measured with Dnmt1 and CRE ab^m substrate (*7*, *9*). In summary, unlike M.HhaI, AdoMet binding by Dnmt1 has minimal effects on its DNA binding affinity.

DISCUSSION

Substrate Inhibition by Dnmt1 Derives from the Turnover-Dependent Relief from Allosteric Inhibition. Our initial interest was to characterize why premethylated and unmethylated DNA show differential substrate inhibition (Figure 4A−C), differences in initial lags (Figure 3A,B) and catalytic rates (Table 1). The increased inhibition observed with increasing concentrations of unmethylated substrate (Figure 4A,B) is consistent with DNA binding at the active site and inhibition site (Figure 10C) as suggested in earlier studies (*8*). The kinetic lag correlates with the extent of substrate inhibition (Figures 3A,B and 4A−C) and is not due to our assay design. Slow relief from enzyme inhibition induced by the start of catalysis is known to lead to an initial lag (*36*, *38*). Thus, we propose that the start of catalysis on unmethylated DNA initiates a slow relief from allosteric inhibition. The initial lag was not routinely described in prior kinetic studies of Dnmt1, in contrast to various forms of substrate inhibition; however, a lag is apparent in some cases (*7*, *26*). The precise nature of this slow relief from allosteric inhibition remains obscure. Plausible driving forces include

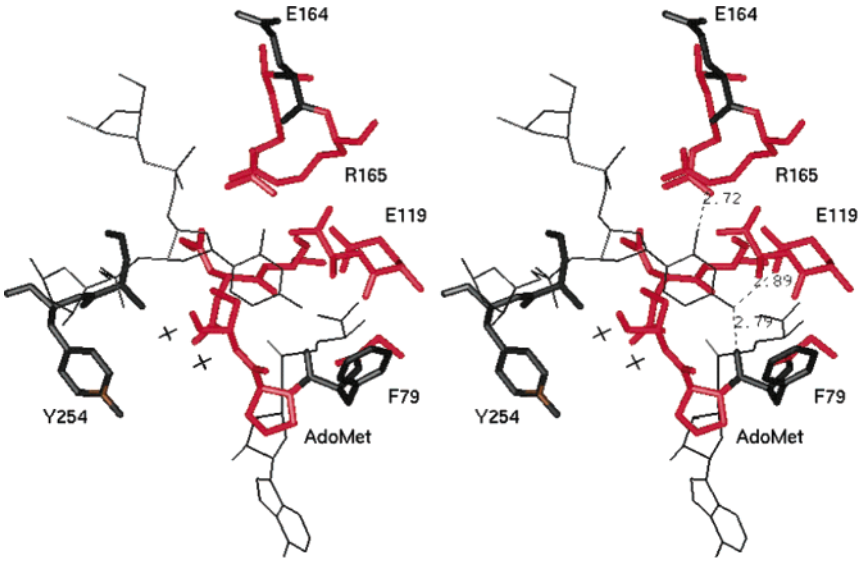

FIGURE 9: Sequence similarity between M.HhaI and Dnmt1 in the active site. Stereo figure (Biosym, InsightII) of M.HhaI active site (pdb code 3MHT, (*53*)). The target base and AdoMet are shown as thin lines, the amino acids forming the catalytic pocket are in bold. The AdoMet structure is taken from pdb file 6MHT (*59*) and superimposed onto the backbone of AdoHcy present in the original structure. Water molecules are indicated as crosses (+). The image was generated in an attempt to construct the Dnmt1 active site by mapping the M.HhaI and Dnmt1 sequences to the M.HhaI structure. The amino acids colored red are identical between M.HhaI and Dnmt1 and belong to the highly conserved domains of the methyltransferase family [motifs IV, VI, and X (*60*)]. Four residues, R^{165}, E^{119}, F^{79}, and C^{81} make direct contact with the target base and mediate the methylation chemistry. Three of these four residues (R, E, and C) are found in M.HhaI and all known metazoan methyltransferases. F^{79} forms a hydrogen bond between the backbone carbonyl oxygen and the C^4 amine of the target base. F^{79} in M.HhaI is replaced by P^{1234} in Dnmt1.

AdoMet binding, DNA release from the site of inhibition, a combination of these two processes, or some other slow conformational change. AdoMet binding is the most likely factor since DNA inhibition is more pronounced at subsaturating AdoMet concentrations (*11*) and since the mutant lacking the functional regulatory domain shows different responses to changes in AdoMet concentration (*11*, *12*) relative to the wild type. In summary, we propose that AdoMet binding to Dnmt1 initiates a slow relief from the allosteric inhibition; a slow relief from allosteric inhibition induced by ligand binding is well documented in the literature (*40* and Figure 10D).

The lack of an initial lag with premethylated substrates (Figures 3A,B and 5A,B) indicates that there is no slow relief from allosteric inhibition at the start of catalysis. The reactions with the premethylated substrate show a pre-steady-state burst (Figure 3) as reported earlier for hemimethylated substrates (*7*). In general, the initial burst indicates that the steps leading to the detection step are faster than the steps following the detection step (p 274 in ref *43*). Thus, the mild pre-steady-state burst indicates that for premethylated substrates the steps leading to intermediate **3A** (Figure 1) are rate-limiting during the initial target base attack, while the subsequent turnovers are partially controlled by formation of intermediate **3A** and by the steps that come after intermediate **3A**. This is consistent with the exchange results (Figures 5 and 6A,B) which showed that with the premethylated substrate the initial target base attack is fast and the rate-limiting step is primarily controlled by the methyltransfer step (Figure 1, **2** → **3A**).

Dnmt1 and M.HhaI Share Similar Reaction Intermediates and Rate-Limiting Steps. We previously used AdoMet analogues and poly(dG-dC) and poly(dI-dC) to study the reaction intermediates and rate-limiting steps of the M.HhaI-catalyzed reaction (*28*). We sought to apply this approach to Dnmt1 to further characterize the enzyme's preference for premethylated DNA and allosteric regulation. The ability of Dnmt1 to catalyze the exchange reaction supports results from studies of 5FC inhibition (*16*) and shows that Dnmt1 has a similar catalytic mechanism as other pyrimidine methyltransferases (Figure 1; *44*). Dnmt1 and M.HhaI share similarities in key aspects of the cytosine C^5 exchange reaction, even though the catalytic rates can differ by 10−100 fold (Table 2). AdoMet analogues modulate the exchange rates by orders of magnitude for both Dnmt1 and M.HhaI (Table 2), indicating that the availability of proximal proton(s) (Figure 2B) in the position of the active methyl moiety is critical (Figure 1). Both Dnmt1 and M.HhaI (Table 2) cause an excess tritium release during the methylation reaction with poly(dI-dC) [and pm-poly(dI-dC), Figure 6A,B], while no excess tritium release is observed with poly(dG-dC) [and pm-poly(dG-dC), Figure 6C]. Finally, we also found that Dnmt1 and M.HhaI show similar proton inventory profiles in the exchange reaction with sinefungin (Figure 7A,B). On the basis of these similarities, we propose that, for both Dnmt1 and M.HhaI, the AdoMet analogues modulate the exchange rates by controlling the proton access at the C^5 on intermediate **2** (Figure 2 and solvent in Figure 9). For both Dnmt1 and M.HhaI, intermediates leading to **1** and **2** accumulate as a dynamic equilibrium (Figure 1B), prior to the slow methyltransfer (Figure 1, **2** → **3A**), or proton-transfer step (Figure 1, **2** → **3B**). If Dnmt1 flips the target base like M.HhaI and other methyltransferases (*45*), the rapid equilibrium would include base flipping and base restacking steps, and the equilibrium between intermediates **1** and **2** (Figure 1B).

In the case of a rapid equilibrium between the steps leading to intermediates **1** and **2**, the observed catalytic rates are not solely dependent on a single rate-limiting event (*28*). Rather, the catalytic rates are simultaneously and independently

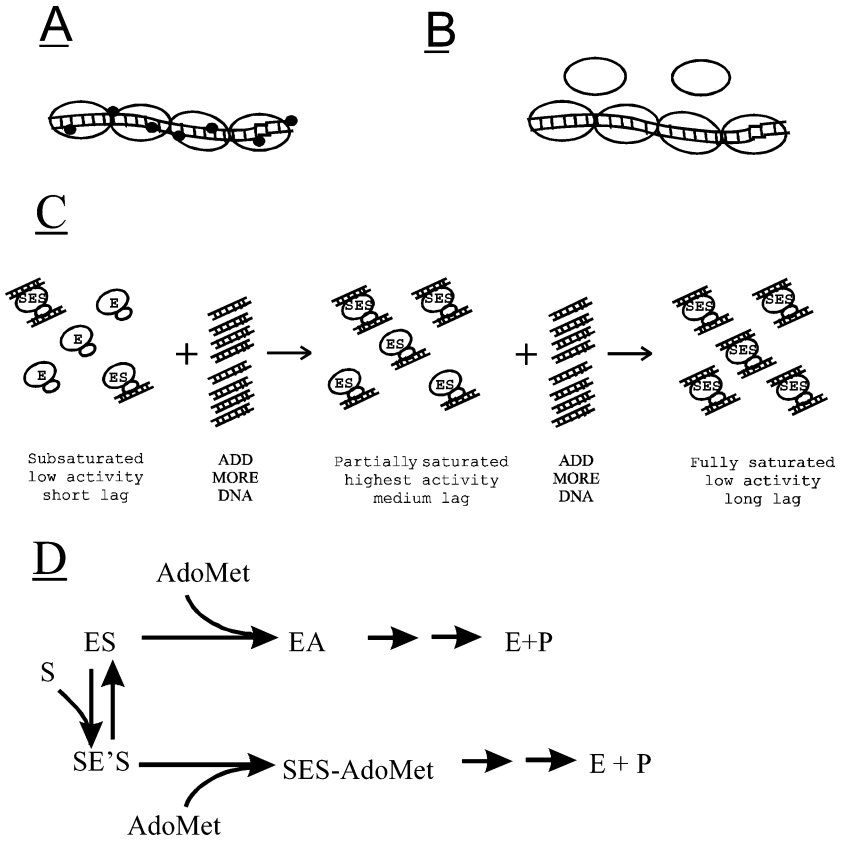

FIGURE 10: (A) Schematic for the interaction between Dnmt1 (oval) and its DNA substrate (rail). Dnmt1 bound on poly(dG-dC) or poly(dI-dC) with ^{5m}C groups (small filled circles) evenly distributed once or twice per enzyme footprint. (B) Given a DNA footprint of approximately 30 bp for Dnmt1 (*7*), a poly(dG-dC) substrate of 120 bp provides 120 CpG methylation sites but only enough flanking DNA to afford binding of approximately four Dnmt1 molecules. Thus, Dnmt1 and DNA are present in close stoichiometric concentrations (see appendix). Substrate concentrations are commonly represented in terms of CpG or CpI sites (*12*−*14*), or in terms of total concentration of long DNA molecules (*7*, *8*, *10*). In both cases, the Dnmt1 to DNA ratios need to be considered (see appendix). (C) The active site (small oval) and the allosteric site (large oval) on Dnmt1 can bind DNA independently (*8*, *11*, *27*). Dnmt1 (E) with DNA bound at the active site (ES), and the active site and the allosteric site (SES) at subsaturating and saturating DNA substrate as in Figures 4A−C. (D) AdoMet binding can initiate a relief from allosteric inhibition and slow transition between the inactive (SE′S) and active form (SES).

regulated by factors that control the concentrations of intermediates **1** and **2** (Figure 1), and by factors that control the methyl transfer (Figure 1, **2** → **3A**) or proton-transfer steps (**2** → **3B**). The methyl transfer rate (Figure 1, **2** → **3A**) is directly proportional to the lifetime of intermediate *2*, which in turn depends on the factors that control the equilibrium between intermediates **1** and **2**, like the pK_a of the active site cysteine (*28*). The lifetime of intermediate **1** is dependent on the ratio between base flipping and the base restacking rates, and the ratio between the conversion rates **1** → **2** and **2** → **1**. For illustration, the base flipping rate can be close to 200 s^{-1} (*46*), while the methyltransfer rate constants are less than 100 h^{-1} (Table 2). If the interchange between the intermediates is predominantly sequential (i.e., A → B → C → D) the base flipping rate can vary by 2 orders of magnitude without significantly affecting the methylation rates ($1/k_{tot} = 1/k_1 + 1/k_2 + 1/k_3$ ... etc.). However, if there is a rapid equilibrium between intermediates (i.e., A ↔ B → C) even a small change in the base flipping vs base restacking rate will affect the equilibrium concentration of intermediate B and consequently the rate of formation for the subsequent intermediates (i.e., d[C]/dt = k[B]$_{eq}$).

In the next few paragraphs, we use the concept of a dynamic equilibrium preceding the slow methyl transfer step to describe the factors that control Dnmt1's catalytic rates. We describe the rate differences between premethylated and unmethylated substrates, the difference between poly(dI-dC) and poly(dG-dC) substrates (Table 2), and the difference between Dnmt1 and M.HhaI (Table 2).

The Dnmt1 Reaction with Premethylated and Unmethylated Substrates Differ in the Rate of Formation of the Covalent Intermediate. The unmethylated and premethylated substrates have different rates of target base attack (Figure 6A,B), yet the methyltransfer step is rate-limiting with both substrates (Figure 6A,B). The tritium exchange rates with sinefungin and premethylated and unmethylated substrates differ by 9-fold (Table 2), yet the proton inventory data show that both reactions are limited by proton transfer at cytosine C^5 (Figure 7A,B). The exchange rates with both premethylated and unmethylated substrates are modulated by orders of magnitude with various AdoMet analogues, yet the rates with the premethylated substrates are uniformly faster (Table 2). In summary, the difference between the unmethylated and premethylated substrates does not derive from the rate-limiting events on intermediate **2** (Figure 1, **2** → **3A** or **2** → **3B**). Rather, the difference derives from changes that favor the accumulation of intermediates **1** and **2** (Figure 6A,B).

Since each target base attack can lead to only one tritium release (Figure 1, **2** → **3B** → **4B**), severalfold higher exchange rates with the premethylated substrates (Figures 5 and 6A,B) indicate that intermediates **1** and **2** are formed

faster with premethylated DNA. In another words, the preference for the premethylated substrate must involve all steps leading to intermediates **1** and **2** (Figure 1B, *45*). Interestingly, the exchange rates with unmethylated DNA are never as fast as with premethylated DNA (Figures 5 and 6A,B), despite the relief from inhibition observed after the lag. Thus, the enzyme's preference for premethylated DNA is determined by the interactions beyond the allosteric site, as earlier studies suggested (*11*).

Variations in the Rates of Covalent Intermediate Formation Account for the Differences between Dnmt1 and M.HhaI and between poly(dI-dC) and poly(dG-dC). Dnmt1's preference for poly(dI-dC) is unusual, resulting in rates comparable to those observed for M.HhaI (Table 2), in contrast to the 2 orders of magnitude difference in pre-steady-state methylation rates with poly(dG-dC) (Table 2 and (*7*)) or other DNA substrates (*15*). The preference for poly(dI-dC) cannot be caused by differences in the allosteric regulation since poly(dI-dC) shows faster rates than pm-poly(dG-dC), even though pm-poly(dG-dC) does not show substrate inhibition. Also, the Dnmt1 mutant lacking the functional allosteric site shows 3−18-fold slower rates with G:C-rich substrates relative to the poly(dI-dC) substrate (*11*, *12*). The preference for poly(dI-dC) substrates is unlikely to result directly from faster catalytic processes at cytosine C^5 (Figure 1, **2** → **3A** or **2** → **3B**) since the reactions with poly(dI-dC) are uniformly faster than poly(dG-dC), even though AdoMet analogues can modulate the exchange rates by 3 orders of magnitude (Table 2). Finally, the proton inventory studies (Figure 7A,B) suggest that all four DNA substrates share the same rate-limiting steps. In summary, our results indicate that the higher catalytic rates with poly(dI-dC) vs poly(dG-dC) (Tables 1 and 2) are not due to the differences in allosteric regulation or in the conversion of intermediates **2** → **3A** or **2** → **3B**. We therefore propose that variations in the accumulation of intermediates **1** and **2** (Figure 1) are most likely responsible. The crystal structures of I:C and G:C base pairs can be superimposed (*47*); however, unlike the G:C base pair, the I:C base pair has only two hydrogen bonds (Figure 2). Thus, a disruption of the I:C base pair during the base flipping process requires less energy, so it is tempting to attribute the faster rates with poly(dI-dC) substrate to a more favorable accumulation of "base-flipped" intermediate (Figure 1B).

Similar to the differences between Dnmt1 reactions with poly(dG-dC) and poly(dI-dC), the difference between Dnmt1 and M.HhaI can be traced to the accumulation of intermediates **1** and **2**. Dnmt1 and M.HhaI show similar rates with poly(dI-dC) substrates (Table 2); however, unlike Dnmt1, M.HhaI shows similar catalytic rates with poly(dI-dC) and poly(dG-dC) substrates (*28*). Thus, the relative slowness of Dnmt1 with poly(dG-dC) substrates accounts for the difference with M.HhaI (Table 2; *15*). On the basis of our exchange reaction results (Figure 2, Table 2) and proton inventory studies (Figure 7), Dnmt1 and M.HhaI share the same mechanism with poly(dI-dC) and poly(dG-dC) once intermediates **1** and **2** are formed. Thus, the uniformly faster rates with M.HhaI (Table 2) must come from early steps leading to intermediates **1** and **2** (Figure 1B) rather than from methyltransfer (Figure 1, **2** → **3A**) or proton-transfer steps (Figure 1, **2** → **3B**).

^{3}H Exchange Reaction and Mutagenic Deamination Share Reaction Intermediates. Mammalian DNA methylation sites are mutation hot spots, which frequently occur in critical cancer-related genes (*48*), as a result of deamination of cytosine to uracil, and 5-methylcytosine to thymine (Figure 1). Bacterial DNA cytosine methyltransferases are known to catalyze the mutagenic deamination of cytosine (*49*), and deamination rates are affected by AdoMet analogues (*50*, *51*). The M.HhaI-catalyzed exchange and deamination reactions are affected by AdoMet analogues in the same fashion (*28*), supporting the idea that the two reactions share similar intermediates (Figure 1, **1** → **2** → **3B** → **3C** → **4C** and refs *44*, *49*−*52*). The deamination reaction is extremely slow and thus difficult to study mechanistically. We studied the Dnmt1-catalyzed exchange reaction to obtain insights into the enzyme's ability to catalyze this, and the related deamination reactions.

Cytosine C^5 methyltransferases need to balance the solvent access at the active site (Figure 9) because the solvent forms part of the obligatory β-elimination step (Figure 1, **3B** → **3C**), and the solvent could lead to mutagenic deamination (Figure 1, **1** → **2** → **3B** → **3C** → **4C**). Intermediates **1** and **2** accumulate prior to the slow methyltransfer step (Figure 6A,B, and ref *28*), thus enhancing the opportunity for solvent access to these intermediates. Intermediate **2** is readily protonated (Figure 1, **2** → **3B**, $pK_a = 11-18$; *29*), thereby increasing the mutagenic deamination process by at least 4 orders of magnitude (*44*). In the case of M.HhaI (*28*), the rate of excess tritium release in the methylation reaction with poly(dI-dC) is enhanced by the positioning of the active site loop (residues 80−99) and enzyme−DNA interactions with the guanine 5′ to the target cytosine. Like M.HhaI, Dnmt1 shows excess tritium release in the methylation reaction with poly(dI-dC), but not with poly(dG-dC) (Figure 6A−C). Thus, for both Dnmt1 and M.HhaI, enzyme interactions with the guanine within the recognition site limit the solvent access to the active site, the exchange reaction, and presumably the mutagenic deamination (Figure 1, **1** → **2** → **3B** → **3C** → **4C**). Aside from the active site loop, the cofactor may also protect intermediates **1** and **2** from solvent (Table 2 and Figure 9). The slow ^{3}H exchange reaction with AdoHcy (Table 2) indicates that for both M.HhaI and Dnmt1, the β-elimination step (Figure 1, **3A**→ **4A**) is unlikely to take place through a direct solvent access to intermediate ***2*** ((*53*, *54*) and Figure 9).

Factors that decrease the lifetime of the extrahelical base are likely to slow down both the exchange and mutagenic deamination reaction. For example, our proposal that Dnmt1 is slower than M.HhaI because intermediates **1** and **2** accumulate to a lesser extent would predict that Dnmt1 is less mutagenic than M.HhaI. In contrast to M.HhaI, the exchange reaction for Dnmt1 is very slow in the absence of cofactor (Table 2). Thus, Dnmt1 is unlikely to form intermediates **1** and **2** (Figure 1) in the absence of the cofactor. Accordingly, Dnmt1 is unlikely to efficiently deaminate cytosine in the absence of the cofactor, which is precisely the condition that shows the most extensive deamination for the majority of bacterial enzymes (*49*−*52*). Unlike M.HhaI (*15*), AdoMet binding by Dnmt1 does not lead to a large change in DNA binding affinity (Figure 8). Thus, cofactor binding by Dnmt1 may not induce the same active site closure as shown for M.HhaI (*33*).

Dnmt1 Is Not Self-Activated by the ^{5m}C Groups Deposited at the Start of the Methylation Reaction on Unmethylated Substrate. It is unclear from the current literature whether Dnmt1's preference for premethylated substrates derives from activation by the premethylated substrates, inhibition by unmethylated substrates, or some combination of these. Here we find that Dnmt1's preference for premethylated substrates derives from allosteric inhibition by unmethylated substrates, rather than allosteric activation by premethylated substrates. First, premethylated DNA (Figure 4C) does not show a sigmoidal curve which is characteristic of substrates that act as allosteric activators (pp 21−29 in ref *38* or pp 203−234 in ref *43*). Second, our observation of a kinetic lag and the resultant "activation" during the sinefungin-mediated exchange reaction (Figure 5) indicates that the faster catalysis following the initial lag *is* not due to activation caused by the deposition of methyl groups at the start of catalysis (Figure 1). Finally, after 10 min of methylation (Figure 6A), the fraction of ^{5m}C becomes comparable to the fraction of ^{5m}C that is present in premethylated poly(dI-dC) (^{5m}C:C = 1:12); yet, we do not see a gradual increase in the tritium release rates to that observed with premethylated poly(dI-dC) (Figure 5, panel B vs A). In summary, at the start of catalysis when there is an excess of unmethylated DNA, the mere presence of ^{5m}C is not enough to induce higher catalytic rates with Dnmt1.

ACKNOWLEDGMENT

We wish to thank UCSB undergraduate students Jamie Witham, Ben Hopkins, and Stephen Fiacco for their excellent help in these experiments. We are grateful to Prof. H. Olin Spivey from Oklahoma State University, Dr. Sriharsa Pradhan at New England Biolabs, and Dr. Albino Bacolla at Texas A&M University for their correspondence during these studies. We are grateful to Prof. Nancy C. Horton at University of Arizona for help in the molecular modeling studies. We gratefully acknowledge Ana M. Ojeda and Dr. Peter Vollmyer for help in purifying Dnmt1.

APPENDIX

Limitation of Michaelis−Menten Kinetics in Dnmt1 Studies and Alternative Approaches in Assay Design. Michaelis−Menten kinetics requires an excess of substrate over enzyme, an initial linear reaction profile, and multiple catalytic turnovers (*43*), all of which are often impossible, or very difficult to achieve with exceptionally slow enzymes such as Dnmt1 (Table 1). The slow catalytic rates require that Dnmt1 concentrations are often comparable to the varied substrate concentration (Figure 10B) (*7*−*9*, *11*, *12*, *24*, *27*, *55*). Thus, competitive and noncompetitive patterns in double reciprocal plots, and the calculated K_m, k_{cat}, and K_i constants reflect the enzyme/DNA ratios and assay design, rather than the kinetic properties of Dnmt1. Accordingly, some of the earlier conclusions regarding the catalytic properties of Dnmt1 should be reevaluated. Similar concerns apply to Dnmt3 studies (*56*). We did not use Michaelis−Menten kinetics to analyze our data or the previously published results (Table 1 and refs *7*, *8*, *10*−*12*, *14*, *24*, *55*). We find a satisfying consensus between different Dnmt1 studies when Michaelis−Menten kinetics is not used for data interpretation (Table 1).

In the earlier studies (*7*, *8*, *10*−*12*, *14*, *24*, *55*), as in Figure 4, at low DNA concentrations (i.e., less than one 30 bp segment per each Dnmt1 molecule, Figure 10 B), there is an excess Dnmt1 (Figure 10C) and catalytic rates are low since only a small fraction of Dnmt1 can bind DNA (ES and SES forms in Figure 10C). Further increases in DNA concentration increase the ES and SES forms and result in higher catalytic rates (Figure 10C). The highest catalytic rates are achieved when the ES form predominates relative to the E, ES, and SES forms (Figure 10C). Once the maximal rates are achieved, a further increase in DNA concentration results primarily in the conversion of the ES to SES form and the visible substrate inhibition (Figure 10C). The fastest rates in Figure 4 and in prior work with similar substrates are attained when 30−60 base pairs of DNA are present per Dnmt1 molecule.

The inability to use Michaelis−Menten kinetics in Dnmt1 studies requires the development of alternative approaches. Briefly, we suggest that Dnmt1 catalytic rates with different DNA substrates should be measured as a function of increasing substrate concentration (as in Figure 4A−C) until full saturation is achieved (as in Figure 10B). This reveals the highest catalytic rates attainable with the tested DNA substrate, and any allosteric inhibition (Figure 4A,B), the lack of allosteric inhibition (Figure 4C), or allosteric activation. If allosteric activation occurs, a change in substrate concentration will give a characteristic sigmoidal change in catalytic rates (*38*, *43*). Studies reporting the allosteric activation of Dnmt1 were not designed to differentiate between the lack of allosteric inhibition (Figure 4C vs Figure 4A,B) from true allosteric activation. Allosteric inhibition was the first and to this day the most consistent and credible evidence of allosteric regulation of Dnmt1 (*7*, *8*, *10*, *11*, *14*, *20*, *26*, *57*). A clear inhibition pattern as observed in Figure 4A,B can be seen only when DNA binding affinity at the allosteric site is higher than the binding affinity at the active site. Thus, in some cases detecting allosteric inhibition can require additional experiments (*8*). When comparing catalytic rates with different DNA substrates it is necessary to separate initial lag effects or other nonlinear effects such as processivity (*41*, *42*) so that different DNA substrates can be compared at equivalent first turnover or multiple turnover stages.

Since it is not possible to measure K_m values for DNA substrates, Dnmt1's preference for DNA substrates has to be determined by measuring binding constants in addition to the catalytic rates. With poly(dG-dC) and poly(dI-dC), formation of ES and SES species is relatively easy to track (Figure 10C). Both substrates show the initial lag even at subsaturating substrate concentration (Figure 3 and Figure 4), indicating that the active site and the allosteric site have similar binding affinities for poly(dG-dC) and poly(dI-dC) (Figure 10C). The change in the lag transition rates (eq 2, k_l) and the catalytic rates as a function of the substrate concentration (Figure 4A,B) can be used with the Adair's equation (*58*) for quantitative determination of the fraction of enzyme molecules present in E, ES, and SES form (Figure 10C), and DNA binding constant for the active site and the allosteric site. Furthermore, experiments such as those shown in Figure 4A−C can be used to test for competitive or uncompetitive inhibitors with regard to DNA substrate. However, such data cannot be analyzed with double recipro-

cal plots, and in such experiments it is necessary to make sure that the chosen substrate and competitor concentration can allow the full range of competition (Figure 10B).

REFERENCES

1. Li, E., Bestor, T. H., and Jaenisch, R. (1992) Targeted mutation of the DNA methyltransferase gene results in embryonic lethality, *Cell 69*, 915−926.
2. Ahuja, N., Li, Q., Mohan, A. L., Baylin, S. B., and Issa, J. P. (1998) Aging and DNA methylation in colorectal mucosa and cancer, *Cancer Res. 58*, 5489−5494.
3. Cunningham, J. M., Christensen, E. R., Tester, D. J., Kim, C. Y., Roche, P. C., Burgart, L. J., and Thibodeau, S. N. (1998) Hypermethylation of the hMLH1 promoter in colon cancer with microsatellite instability, *Cancer Res. 58*, 3455−3460.
4. Kane, M. F., Loda, M., Gaida, G. M., Lipman, J., Mishra, R., Goldman, H., Jessup, J. M., and Kolodner, R. (1997) Methylation of the hMLH1 promoter correlates with lack of expression of hMLH1 in sporadic colon tumors and mismatch repair-defective human tumor cell lines, *Cancer Res. 57*, 808−811.
5. Veigl, M. L., Kasturi, L., Olechnowicz, J., Ma, A. H., Lutterbaugh, J. D., Periyasamy, S., Li, G. M., Drummond, J., Modrich, P. L., Sedwick, W. D., and Markowitz, S. D. (1998) Biallelic inactivation of hMLH1 by epigenetic gene silencing, a novel mechanism causing human MSI cancers, *Proc. Natl. Acad. Sci., U.S.A. 95*, 8698−8702.
6. Egger, G., Liang, G., Aparicio, A., and Jones, P. A. (2004) Epigenetics in human disease and prospects for epigenetic therapy, *Nature 429*, 457−463.
7. Flynn, J., Glickman, J. F., and Reich, N. O. (1996) Murine DNA cytosine-C5 methyltransferase: pre-steady- and steady-state kinetic analysis with regulatory DNA sequences, *Biochemistry 35*, 7308−7315.
8. Flynn, J., Fang, J. Y., Mikovits, J. A., and Reich, N. O. (2003) A potent cell-active allosteric inhibitor of murine DNA cytosine C5 methyltransferase, *J. Biol. Chem. 278*, 8238−8243.
9. Flynn, J., Azzam, R., and Reich, N. (1998) DNA binding discrimination of the murine DNA cytosine-C5 methyltransferase, *J. Mol. Biol. 279*, 101−116.
10. Flynn, J., and Reich, N. (1998) Murine DNA (cytosine-5-)-methyltransferase: steady-state and substrate trapping analyses of the kinetic mechanism, *Biochemistry 37*, 15162−15169.
11. Bacolla, A., Pradhan, S., Larson, J. E., Roberts, R. J., and Wells, R. D. (2001) Recombinant human DNA (cytosine-5) methyltransferase. III. Allosteric control, reaction order, and influence of plasmid topology and triplet repeat length on methylation of the fragile X CGG.CCG sequence, *J. Biol. Chem. 276*, 18605−18613.
12. Bacolla, A., Pradhan, S., Roberts, R. J., and Wells, R. D. (1999) Recombinant human DNA (cytosine-5) methyltransferase. II. Steady-state kinetics reveal allosteric activation by methylated DNA, *J. Biol. Chem. 274*, 33011−33019.
13. Pradhan, S., and Roberts, R. J. (2000) Hybrid mouse-prokaryotic DNA (cytosine-5) methyltransferases retain the specificity of the parental C-terminal domain, *EMBO J. 19*, 2103−2114.
14. Pradhan, S., Bacolla, A., Wells, R. D., and Roberts, R. J. (1999) Recombinant human DNA (cytosine-5) methyltransferase. I. Expression, purification, and comparison of de novo and maintenance methylation, *J. Biol. Chem. 274*, 33002−33010.
15. Lindstrom, W. M., Jr., Flynn, J., and Reich, N. O. (2000) Reconciling structure and function in HhaI DNA cytosine-C-5 methyltransferase, *J. Biol. Chem. 275*, 4912−4919.
16. Yoder, J. A., Soman, N. S., Verdine, G. L., and Bestor, T. H. (1997) DNA (cytosine-5)-methyltransferases in mouse cells and tissues. Studies with a mechanism-based probe, *J. Mol. Biol. 270*, 385−395.
17. Pradhan, S., and Esteve, P. O. (2003) Mammalian DNA (cytosine-5) methyltransferases and their expression, *Clin. Immunol. 109*, 6−16.
18. Lauster, R., Trautner, T. A., and Noyer-Weidner, M. (1989) Cytosine-specific type II DNA methyltransferases. A conserved enzyme core with variable target-recognizing domains, *J. Mol. Biol. 206*, 305−312.
19. Glickman, J. F., Pavlovich, J. G., and Reich, N. O. (1997) Peptide mapping of the murine DNA methyltransferase reveals a major phosphorylation site and the start of translation, *J. Biol. Chem. 272*, 17851−17857.
20. Bestor, T. H. (1992) Activation of mammalian DNA methyltransferase by cleavage of a Zn binding regulatory domain, *EMBO J. 11*, 2611−2617.
21. Bestor, T. H., and Verdine, G. L. (1994) DNA methyltransferases, *Curr. Opin. Cell Biol. 6*, 380−389.
22. Chuang, L. S., Ian, H. I., Koh, T. W., Ng, H. H., Xu, G., and Li, B. F. (1997) Human DNA-(cytosine-5) methyltransferase-PCNA complex as a target for p21WAF1, *Science 277*, 1996−2000.
23. Leonhardt, H., Page, A. W., Weier, H. U., and Bestor, T. H. (1992) A targeting sequence directs DNA methyltransferase to sites of DNA replication in mammalian nuclei, *Cell 71*, 865−873.
24. Aubol, B. E., and Reich, N. O. (2003) Murine DNA cytosine C(5)-methyltransferase: in vitro studies of de novo methylation spreading, *Biochem. Biophys. Res. Commun. 310*, 209−214.
25. Jones, P. A., and Takai, D. (2001) The role of DNA methylation in mammalian epigenetics, *Science 293*, 1068−1070.
26. Pedrali-Noy, G., and Weissbach, A. (1986) Mammalian DNA methyltransferases prefer poly(dI-dC) as substrate, *J. Biol. Chem. 261*, 7600−7602.
27. Pradhan, S., and Esteve, P. O. (2003) Allosteric activator domain of maintenance human DNA (cytosine-5) methyltransferase and its role in methylation spreading, *Biochemistry 42*, 5321−5332.
28. Svedruzic, Z. M., and Reich, N. O. (2004) The Mechanism of Target Base Attack in DNA Cytosine Carbon 5 Methylation, *Biochemistry 43*, 11460−11473.
29. Perakyla, M. (1998) A Model Study of the Enzyme-Catalyzed Cytosine Methylation Using ab Initio Quantum Mechanical and Density Functional Theory Calculations: pK_a of the Cytosine N3 in the Intermediates and Transition States of the Reaction, *J. Am. Chem. Soc. 120*, 12895−12902.
30. Brueckner, B., and Lyko, F. (2004) DNA methyltransferase inhibitors: old and new drugs for an epigenetic cancer therapy, *Trends Pharmacol. Sci. 25*, 551−554.
31. Reich, N. O., and Everett, E. A. (1990) Identification of peptides involved in *S*-adenosylmethionine binding in the EcoRI DNA methylase. Photoaffinity laveling with 8-azido-S-adenosylmethionine, *J. Biol. Chem. 265*, 8929−8934.
32. Xu, G., Flynn, J., Glickman, J. F., and Reich, N. O. (1995) Purification and stabilization of mouse DNA methyltransferase, *Biochem. Biophys. Res. Commun. 207*, 544−551.
33. Klimasauskas, S., Kumar, S., Roberts, R. J., and Cheng, X. (1994) HhaI methyltransferase flips its target base out of the DNA helix, *Cell 76*, 357−369.
34. Wu, J. C., and Santi, D. V. (1987) Kinetic and catalytic mechanism of HhaI methyltransferase, *J. Biol. Chem. 262*, 4778−4786.
35. Johnson, K. A. (1992) in *The Enzymes* (Boyer, P. A., Ed.), Academic Press, Inc., New York.
36. Frieden, C. (1970) Kinetic aspects of regulation of metabolic processes. The hysteretic enzyme concept, *J. Biol. Chem. 245*, 5788−5799.
37. Quinn, D. M., and Sutton, L. D. (1991) in *Enzyme Mechanisam from Isotope Effects* (Cook, P. F., Ed.) pp 73−126, CRC Press, Boca Raton, FL.
38. Tipton, K. F. (2002) in *Practical Approach* (Eisenthal, R., and Danson, M. J., Eds.) p 282, Oxford University Press.
39. Klimasauskas, S., Szyperski, T., Serva, S., and Wuthrich, K. (1998) Dynamic modes of the flipped-out cytosine during HhaI methyltransferase-DNA interactions in solution, *EMBO J. 17*, 317−324.
40. Neet, K. E. (1995) Cooperativity in enzyme function: equilibrium and kinetic aspects, *Methods Enzymol. 249*, 519−567.
41. Vilkaitis, G., Suetake, I., Klimasauskas, S., and Tajima, S. (2005) Processive Methylation of Hemimethylated CpG Sites by Mouse Dnmt1 DNA Methyltransferase, *J. Biol. Chem. 280*, 64−72.
42. Hermann, A., Goyal, R., and Jeltsch, A. (2004) The Dnmt1 DNA-(cytosine-C5)-methyltransferase methylates DNA processively with high preference for hemimethylated target sites, *J. Biol. Chem. 279*, 48350−48359.
43. Cornish-Bowden, A. (1999) *Fundamentals of Enzyme Kinetics*, Portland Press.
44. Ivanetich, K. M., and Santi, D. V. (1992) 5,6-dihydropyrimidine adducts in the reactions and interactions of pyrimidines with proteins, *Prog. Nucleic Acid Res. Mol. Biol. 42*, 127−156.
45. Roberts, R. J., and Cheng, X. (1998) Base flipping, *Annu. Rev. Biochem. 67*, 181−198.
46. Allan, B. W., Reich, N. O., and Beechem, J. M. (1999) Measurement of the absolute temporal coupling between DNA binding and base flipping, *Biochemistry 38*, 5308−5314.

47. Kumar, V. D., Harrison, R. W., Andrews, L. C., and Weber, I. T. (1992) Crystal structure at 1.5-Å resolution of d(CGCICICG), an octanucleotide containing inosine, and its comparison with d(CGCG) and d(CGCGCG) structures, *Biochemistry 31*, 1541−1550.
48. Pfeifer, G. P., Tang, M., and Denissenko, M. F. (2000) in *DNA Methylation and Cancer* (Johns, P. A., and Vogt, P. K., Eds.) pp 1−19, Springer-Verlag.
49. Shen, J. C., Rideout, W. M. d., and Jones, P. A. (1992) High-frequency mutagenesis by a DNA methyltransferase, *Cell 71*, 1073−1080.
50. Zingg, J. M., Shen, J. C., and Jones, P. A. (1998) Enzyme-mediated cytosine deamination by the bacterial methyltransferase M.MspI, *Biochem. J. 332*, 223−230.
51. Zingg, J. M., Shen, J. C., Yang, A. S., Rapoport, H., and Jones, P. A. (1996) Methylation inhibitors can increase the rate of cytosine deamination by (cytosine-5)-DNA methyltransferase, *Nucleic Acids Res*. *24*, 3267−3275.
52. Gabbara, S., Sheluho, D., and Bhagwat, A. S. (1995) Cytosine methyltransferase from *Escherichia coli* in which active site cysteine is replaced with serine is partially active, *Biochemistry 34*, 8914−8923.
53. O'Gara, M., Klimasauskas, S., Roberts, R. J., and Cheng, X. (1996) Enzymatic C5-cytosine methylation of DNA: mechanistic implications of new crystal structures for HhaL methyltransferase-DNA-AdoHcy complexes, *J. Mol. Biol. 261*, 634−645.
54. Lau, E. Y., and Bruice, T. C. (1999) Active site dynamics of the HhaI methyltransferase: insights from computer simulation, *J. Mol. Biol. 293*, 9−18.
55. Fatemi, M., Hermann, A., Pradhan, S., and Jeltsch, A. (2001) The activity of the murine DNA methyltransferase Dnmt1 is controlled by interaction of the catalytic domain with the N-terminal part of the enzyme leading to an allosteric activation of the enzyme after binding to methylated DNA, *J. Mol. Biol. 309*, 1189−1199.
56. Yokochi, T., and Robertson, K. D. (2002) Preferential methylation of unmethylated DNA by Mammalian de novo DNA methyltransferase Dnmt3a, *J. Biol. Chem. 277*, 11735−11745.
57. Glickman, J. F., and Reich, N. O. (1994) Baculovirus-mediated high level expression of a mammalian DNA methyltransferase, *Biochem. Biophys. Res. Commun. 204*, 1003−1008.
58. vanHolde, K. E., Johnson, W. C., and Ho, P. S. (1998) *Principles of Physical Biochemistry*, 1st ed., Prentice Hall.
59. Kumar, S., Horton, J. R., Jones, G. D., Walker, R. T., Roberts, R. J., and Cheng, X. (1997) DNA containing 4′-thio-2′-deoxycytidine inhibits methylation by HhaI methyltransferase, *Nucleic Acids Res. 25*, 2773−2783.
60. Kumar, S., Cheng, X., Klimasauskas, S., Mi, S., Posfai, J., Roberts, R. J., and Wilson, G. G. (1994) The DNA (cytosine-5) methyltransferases, *Nucleic Acids Res. 22*, 1−10.

BI050295Z